AMERICAN SOCIETY FOR MICROBIOLOGY | mSphere®

RESEARCH ARTICLE
Host-Microbe Biology

Calcium Binding Protein Ncs1 Is Calcineurin Regulated in *Cryptococcus neoformans* and Essential for Cell Division and Virulence

Eamim Daidrê Squizani,[a] Júlia Catarina Vieira Reuwsaat,[a] Sophie Lev,[b,c,d] Heryk Motta,[a] Julia Sperotto,[a] Keren Kaufman-Francis,[b,c,d] Desmarini Desmarini,[b,c,d] Marilene Henning Vainstein,[a] Charley Christian Staats,[a] Julianne T. Djordjevic,[b,c,d] Lívia Kmetzsch[a]

[a]Centro de Biotecnologia, Universidade Federal do Rio Grande do Sul, UFRGS, Porto Alegre, Rio Grande do Sul, Brazil
[b]Centre for Infectious Diseases and Microbiology, The Westmead Institute for Medical Research, Sydney, New South Wales, Australia
[c]Sydney Medical School-Westmead, University of Sydney, Sydney, New South Wales, Australia
[d]Marie Bashir Institute for Infectious Diseases and Biosecurity, University of Sydney, Sydney, New South Wales, Australia

Julianne T. Djordjevic and Lívia Kmetzsch share senior authorship.

ABSTRACT Intracellular calcium (Ca^{2+}) is crucial for signal transduction in *Cryptococcus neoformans*, the major cause of fatal fungal meningitis. The calcineurin pathway is the only Ca^{2+}-requiring signaling cascade implicated in cryptococcal stress adaptation and virulence, with Ca^{2+} binding mediated by the EF-hand domains of the Ca^{2+} sensor protein calmodulin. In this study, we identified the cryptococcal ortholog of neuronal calcium sensor 1 (Ncs1) as a member of the EF-hand superfamily. We demonstrated that Ncs1 has a role in Ca^{2+} homeostasis under stress and nonstress conditions, as the *ncs1*Δ mutant is sensitive to a high Ca^{2+} concentration and has an elevated basal Ca^{2+} level. Furthermore, *NCS1* expression is induced by Ca^{2+}, with the Ncs1 protein adopting a punctate subcellular distribution. We also demonstrate that, in contrast to the case with *Saccharomyces cerevisiae*, *NCS1* expression in *C. neoformans* is regulated by the calcineurin pathway via the transcription factor Crz1, as *NCS1* expression is reduced by FK506 treatment and *CRZ1* deletion. Moreover, the *ncs1*Δ mutant shares a high temperature and high Ca^{2+} sensitivity phenotype with the calcineurin and calmodulin mutants (*cna1*Δ and *cam1*Δ), and the *NCS1* promoter contains two calcineurin/Crz1-dependent response elements (CDRE1). Ncs1 deficiency coincided with reduced growth, characterized by delayed bud emergence and aberrant cell division, and hypovirulence in a mouse infection model. In summary, our data show that Ncs1 has a significant role as a Ca^{2+} sensor in *C. neoformans*, working with calcineurin to regulate Ca^{2+} homeostasis and, consequently, promote fungal growth and virulence.

IMPORTANCE *Cryptococcus neoformans* is the major cause of fungal meningitis in HIV-infected patients. Several studies have highlighted the important contributions of Ca^{2+} signaling and homeostasis to the virulence of *C. neoformans*. Here, we identify the cryptococcal ortholog of neuronal calcium sensor 1 (Ncs1) and demonstrate its role in Ca^{2+} homeostasis, bud emergence, cell cycle progression, and virulence. We also show that Ncs1 function is regulated by the calcineurin/Crz1 signaling cascade. Our work provides evidence of a link between Ca^{2+} homeostasis and cell cycle progression in *C. neoformans*.

KEYWORDS calcium binding protein, calcium sensor, *Cryptococcus neoformans*, calcium signaling

Citation Squizani ED, Reuwsaat JCV, Lev S, Motta H, Sperotto J, Kaufman-Francis K, Desmarini D, Vainstein MH, Staats CC, Djordjevic JT, Kmetzsch L. 2020. Calcium binding protein Ncs1 is calcineurin regulated in *Cryptococcus neoformans* and essential for cell division and virulence. mSphere 5:e00761-20. https://doi.org/10.1128/mSphere.00761-20.

Editor Aaron P. Mitchell, University of Georgia

Address correspondence to Julianne T. Djordjevic, julianne.djordjevic@sydney.edu.au, or Lívia Kmetzsch, liviak@cbiot.ufrgs.br.

Received 23 July 2020
Accepted 28 August 2020
Published 9 September 2020

Cryptococcus neoformans is a basidiomycetous pathogenic yeast found mostly in soil and bird droppings (1–3). This pathogen is the etiological agent of cryptococcosis, which affects mainly immunocompromised individuals. This disease affects more than 220,000 HIV-infected patients per year, resulting in more than 180,000 deaths worldwide (3, 4). The lung infection is initiated following the inhalation of small desiccated cells or spores. The infection can then spread via the bloodstream to the central nervous system, causing meningoencephalitis, which is the primary cause of death (1, 5). To survive within the host environment, *C. neoformans* produces several virulence determinants, including a polysaccharide capsule, the pigment melanin, secreted enzymes (6–9), and extracellular vesicles (10). *C. neoformans* survival in the host is possible only due to its ability to grow at 37°C and is also aided by its capacity to survive within phagocytic mammalian cells (1, 11–15).

Fungal fitness and survival in the host environment are controlled by numerous signaling pathways, including those that are regulated by intracellular Ca^{2+}, which is an essential second messenger in eukaryotic cells (16–19). An increase in cytosolic Ca^{2+} is monitored by Ca^{2+} sensor proteins that, upon binding to Ca^{2+}, change their conformation and transduce signals onto downstream targets (20, 21). An important Ca^{2+} sensor in fungal cells is calmodulin, which is a component of the calcineurin signaling pathway. Ca^{2+}-induced conformational change in calmodulin activates the serine-threonine phosphatase calcineurin. Calcineurin then mediates the regulation of several cellular responses by initiating changes in the phosphorylation status of its downstream targets (18, 22, 23). A major target of cryptococcal calcineurin is the transcription factor Crz1, which regulates the expression of genes involved in stress response and in the maintenance of cell wall integrity (24, 25). In *C. neoformans*, the calcineurin pathway is also essential for growth at 37°C, sexual reproduction, and virulence (26); in *Saccharomyces cerevisiae*, it is required for cell cycle progression (27).

Given that high levels of cellular Ca^{2+} can be toxic, Ca^{2+} homeostasis is strictly regulated by several proteins acting as transporters, channels, or pumps (28). In *C. neoformans*, these proteins include Cch1, a Ca^{2+} voltage-gated channel essential for virulence, and Mid1, a stretch-activated Ca^{2+}-channel, both found in the plasma membrane (19, 29). Other cryptococcal calcium transporters that also promote virulence include the Ca^{2+} ATPase Ecal, found in sarcoplasmic/endoplasmic reticulum, and the H^+/Ca^{2+} exchanger protein Vcx1 and the Ca^{2+} ATPase Pmc1, both localized on vacuolar membranes and responsible for Ca^{2+} storage (30–33). Pmc1 is also required for *C. neoformans* transmigration through the blood-brain barrier (BBB), proving that Pmc1-regulated Ca^{2+} homeostasis is crucial for disease progression (33).

Despite the importance of Ca^{2+} homeostasis-related proteins in fungal cell fitness and virulence, with the exception of calmodulin, little is known about the function of other calcium binding proteins (CBPs) that act as Ca^{2+} sensors in *C. neoformans*. One such protein is neuronal calcium sensor 1 (Ncs1). Ncs1 orthologs in other fungi have roles in cell growth and viability, tolerance to Ca^{2+} (34–41), membrane sterol distribution, and expression of Ca^{2+} transporter genes (41). In this study, we identified and characterized the Ncs1 ortholog in *C. neoformans*. Using gene deletion and *in silico* analysis, we investigated the role of Ncs1 in Ca^{2+} homeostasis, growth, stress tolerance, and virulence and whether Ncs1 function is linked to the calcineurin pathway.

RESULTS

Identification of the Ncs1 ortholog in *C. neoformans*. CBPs are either predominantly intrinsic membrane proteins that transport Ca^{2+} through membranes or Ca^{2+}-modulated proteins, mainly represented by Ca^{2+} sensors involved in signal transduction (21, 28). The latter include calmodulin and calcineurin, which harbor the calcium-binding (EF-hand) domain. Both proteins have been well studied in eukaryotic cells, including *C. neoformans* (25, 26, 42). However, calmodulin is the only intracellular calcium sensor characterized so far in *C. neoformans*. Considering the number and complexity of processes regulated by Ca^{2+}, we sought to identify other CBPs in the EF-hand superfamily with Ca^{2+} sensor functions. In this context, we searched for the

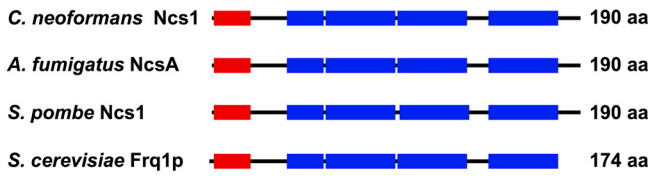

FIG 1 Identification of Ncs1 as a putative calcium binding protein in *C. neoformans*. Comparative *in silico* analysis of *C. neoformans* Ncs1 (CNAG_03370), *Aspergillus fumigatus* NcsA (Afu6g14240), *Schizosaccharomyces pombe* Ncs1 (SPAC18B11.04), and *S. cerevisiae* Frq1 (YDR373W) amino acid (aa) sequences indicates the presence and positions of the four EF-hand domains (blue bars) and the N-terminal myristoylation domain (red bars).

neuronal calcium sensor 1 (Ncs1) homolog in *C. neoformans*, given that this protein is important for Ca^{2+} regulated processes in a variety of eukaryotic cells (43).

For this purpose, we performed an *in silico* analysis at FungiDB to identify the *NCS1* coding sequence in the *C. neoformans* H99 genome (CNAG_03370). Ncs1 is well conserved in eukaryotes, with orthologs sharing common regions, such as EF-hand domains and a myristoylation motif. Our analysis revealed that *C. neoformans* Ncs1 contains four predicted EF-hand domains that span the full length of the protein (Fig. 1). Moreover, the presence of an N-terminal myristoylation motif was identified using the NMT-themyr predictor database. Myristoylation, a lipid modification conserved among eukaryotic Ncs1 proteins (44), is important for cell signaling, protein-protein interaction, and protein targeting to endomembrane systems and the plasma membrane (45). Comparative analysis of the *C. neoformans* Ncs1 protein sequence with the products encoded by *Aspergillus fumigatus NCSA* (Afu6g14240), *Schizosaccharomyces pombe NCS1* (SPAC18B11.04), and *S. cerevisiae FRQ1* (YDR373W), which are already functionally characterized (34, 40, 41), revealed high degrees of amino acid sequence similarity (86, 87, and 81%, respectively) (Fig. 1).

Disruption of the *NCS1* gene affects *C. neoformans* traits associated with calcium homeostasis. Calcium sensor proteins measure fluctuations in free cytosolic Ca^{2+} and transduce the signal to downstream effectors (41, 42, 46). To determine whether Ncs1 plays a similar role in *C. neoformans*, we obtained a *NCS1* gene knockout strain (*ncs1*Δ) from Madhani's mutant collection (47) and generated an *NCS1* reconstituted (*ncs1*Δ::*NCS1*) strain (see Fig. S1 in the supplemental material) using the *ncs1*Δ background. We then evaluated the ability of these mutant strains to grow under different stresses. We initially chose high Ca^{2+} concentration (to alter Ca^{2+} homeostasis) and high temperatures (37°C and 39°C), as the calcineurin (*cna1*Δ) and calmodulin (*cam1*Δ) mutants were shown to be sensitive under these growth conditions (24, 25, 42). We observed impaired *ncs1*Δ strain growth in high Ca^{2+} levels and at 39°C but not at 37°C; these growth defects were restored to wild-type (WT) levels in the *ncs1*Δ::*NCS1* strain (Fig. 2). Lower Ca^{2+} concentrations (ranging from 1 to 20 mM $CaCl_2$) did not influence *ncs1*Δ strain growth (data not shown). Other traits associated with the

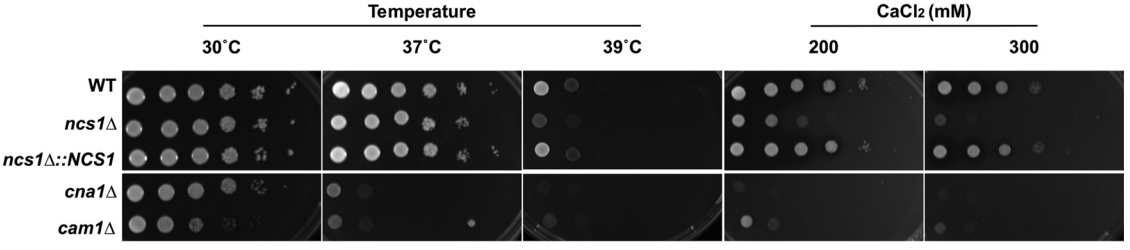

FIG 2 Disruption of *NCS1* leads to stress sensitivity in *C. neoformans*. Spot plate assays of the WT, *ncs1*Δ mutant, and *ncs1*Δ::*NCS1* complemented cells were performed on YPD agar. The plates were incubated at 30°C (control for normal growth), 37°C, or 39°C and under stress induced by Ca^{2+} (200 mM or 300 mM $CaCl_2$ at 30°C). The calcineurin (*cna1*Δ) and calmodulin (*cam1*Δ) mutants were included as controls, separated by a thin white line that indicates noncontiguous portions of the same image. All assays were conducted for 48 h.

Ca^{2+}-calcineurin pathway, such as growth in the presence of cell wall-perturbing agents (calcofluor white and Congo red) and osmotic stress (1 M NaCl) were evaluated in the *ncs1*Δ null mutant, with no effect observed (Fig. S2).

We also evaluated whether the level of free intracellular Ca^{2+} in *C. neoformans* is affected in the absence of Ncs1. Relative to the WT strain, the *ncs1*Δ mutant had a higher basal level of free cytosolic Ca^{2+}, which was reduced to WT levels in the *ncs1*Δ::*NCS1* strain. This high-Ca^{2+}-level phenotype was shared with that observed for the *cna1*Δ and *cam1*Δ mutant strains (Fig. 3A). In *S. pombe*, Ncs1 physically interacts with the Mid1 ortholog, Yam8, which is a stretch-activated Ca^{2+} channel. *S. pombe YAM8* gene disruption in the *ncs1*Δ background restored the Ca^{2+}-sensitive phenotype (35). In this study, the authors proposed that Ncs1 negatively regulates the Yam8 calcium channel. We therefore investigated whether the high-affinity Mid1-Cch1 calcium channel complex (48, 49) is responsible for the increased intracellular Ca^{2+} observed in the *ncs1*Δ mutant. Specifically, we used real-time reverse transcription-quantitative PCR (RT-qPCR) to compare the expressions of *MID1* and *CCH1* in WT and *ncs1*Δ grown in yeast extract-peptone-dextrose (YPD) with or without 100 mM $CaCl_2$ for 24 h. The transcript levels of both genes increased by approximately 3-fold in the *ncs1*Δ mutant strain, but only following growth in the presence of 100 mM $CaCl_2$ (Fig. 3B). No differences in *CCH1* and *MID1* expression was observed in the WT and the *ncs1*Δ strain grown in YPD without $CaCl_2$ (Fig. 3B), suggesting that the Mid1-Cch1 complex, which imports Ca^{2+} into the cytosol (29, 48), is not the source of extra Ca^{2+} in the *ncs1*Δ mutant. In further support of this, we generated a *mid1*Δ *ncs1*Δ double mutant in *C. neoformans* and found that increased intracellular Ca^{2+} accumulation and Ca^{2+} sensitivity persisted in this mutant (Fig. S3). Despite these findings, we cannot rule out the involvement of other low-affinity calcium channels in contributing to the increased intracellular Ca^{2+} observed in the *ncs1*Δ mutant.

We also C-terminally tagged Ncs1 with green fluorescent protein (GFP) (*NCS1*::*GFP*) to assess Ncs1 subcellular localization. Faint, predominantly cytosolic, Ncs1 fluorescence was observed when the strain was cultured in the absence of Ca^{2+}. However, the fluorescence was higher than that observed for the nonfluorescent WT control strain (Fig. 3C). Ncs1 fluorescence became more intense following culture in the presence of Ca^{2+} (100 mM $CaCl_2$), with Ncs1 adopting a more punctate staining pattern: 24.5% ± 1.1% and 36.3% ± 3.0% of the cell population displayed puncta in the absence (MM) and presence (MM + $CaCl_2$) of Ca^{2+}, respectively ($P = 0.013$, Welch's test with ≥200 cells per sample) (Fig. 3C). Increased Ncs1 fluorescence in the presence of Ca^{2+} correlated with higher expression of *NCS1* by the *NCS1*::*GFP* strain under the same condition (Fig. 3D). Taken together, these results suggest that Ncs1 responds to increase in intracellular Ca^{2+} levels and participates in the regulation of calcium homeostasis in *C. neoformans*.

***NCS1* is a calcineurin-Crz1 responsive gene.** Given that *NCS1* is a Ca^{2+}-responsive gene in *C. neoformans* (Fig. 3D), we investigated whether *NCS1* expression is regulated by the calcineurin signaling pathway via the transcription factor Crz1. *NCS1* expression was analyzed in the presence and absence of the calcineurin inhibitor FK506 (Fig. 4A) and in the WT and *crz1*Δ mutant (Fig. 4B). The results demonstrated that FK506 treatment reduced *NCS1* transcription in the WT (Fig. 4A) and that *NCS1* expression was downregulated in the *crz1*Δ mutant at 25°C and 37°C (Fig. 4B). In further support of *NCS1* being a Crz1 target, we identified two Crz1-binding consensus motifs (50) in the putative *NCS1* regulatory region encompassing the 1,000-nucleotide sequence upstream of the transcription start site (Fig. 4C). These findings provide evidence that Ncs1 and calcineurin work together to regulate Ca^{2+} homeostasis.

Ncs1 activity is essential for *C. neoformans* virulence. As proven in other studies, the disruption of Ca^{2+} homeostasis components is important for cryptococcal pathogenicity (29–33, 51). To determine whether disruption of Ncs1-mediated calcium homeostasis also contributes to pathogenicity, we compared the virulence of the *ncs1*Δ mutant strain to that observed for the WT and *ncs1*Δ::*NCS1* strains in a mouse inhalation

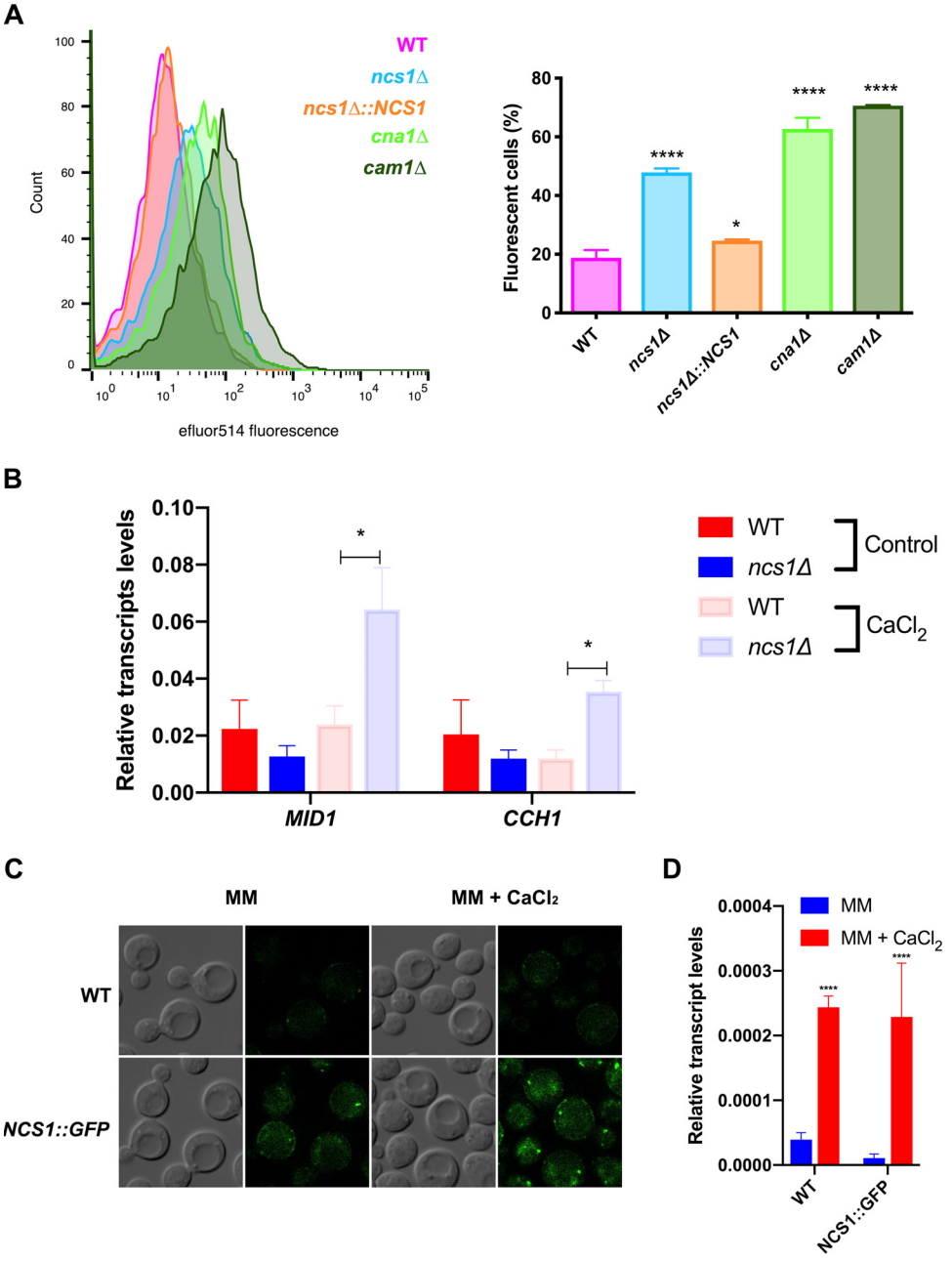

FIG 3 Cryptococcal Ncs1 is associated with Ca^{2+} homeostasis. (A) The basal levels of free intracellular Ca^{2+} in WT, *ncs1*Δ, *ncs1*Δ::*NCS1*, *cna1*Δ, and *cam1*Δ mutant cells were quantified by flow cytometry following staining with the calcium-specific dye Fluo-4-AM. The left side represents the histogram of Fluo-4-AM emitted fluorescence of indicated strains cultivated in YPD medium at 30° C. The right side represents the percentage of gated fluorescent cells ± standard deviation (three biological replicates). Mean values were compared using one-way ANOVA and Dunnett's *post hoc* test. Statistical significance is represented as follows: ****, $P < 0.0001$, and *, $P < 0.05$. (B) The transcript levels of genes encoding the calcium transporters, *CCH1* and *MID1*, were evaluated using RT-qPCR. The WT and *ncs1*Δ strains (10^6 cells/ml) were incubated in YPD for 16 h with shaking, either at 37°C (control) or at 37°C supplemented with Ca^{2+} (100 mM $CaCl_2$). RNA was extracted and cDNA synthesized. Each bar represents the mean ± the standard deviation ($n = 3$) for each gene in each strain normalized to actin. Statistical analysis was performed using Student's *t* test (*, $P < 0.05$). (C) Ncs1 was tagged with GFP (*NCS1*::*GFP*), and the effect of $CaCl_2$ supplementation on Ncs1 production and subcellular localization was assessed by fluorescence microscopy. YPD overnight cultures of the WT (autofluorescence background control) and the *NCS1*::*GFP* strain were washed twice with water and used to seed on minimal medium (MM) or MM supplemented with Ca^{2+} (100 mM $CaCl_2$) at an OD_{600} of 1. The cultures were further incubated for 4 h at 30°C prior to visualization. DIC and green fluorescent images are included. (D) The cultures prepared for panel C were also used to extract RNA and perform RT-qPCR to assess the effect of Ca^{2+} on the transcript levels of *NCS1*, normalized to actin. Statistical analysis was performed using one-way ANOVA with Tukey *post hoc* test. Comparisons were conducted between WT cells grown in the absence or in the presence of Ca^{2+} or between *NCS1*::*GFP* cells grown in the absence or in the presence of Ca^{2+}. ****, $P < 0.0001$.

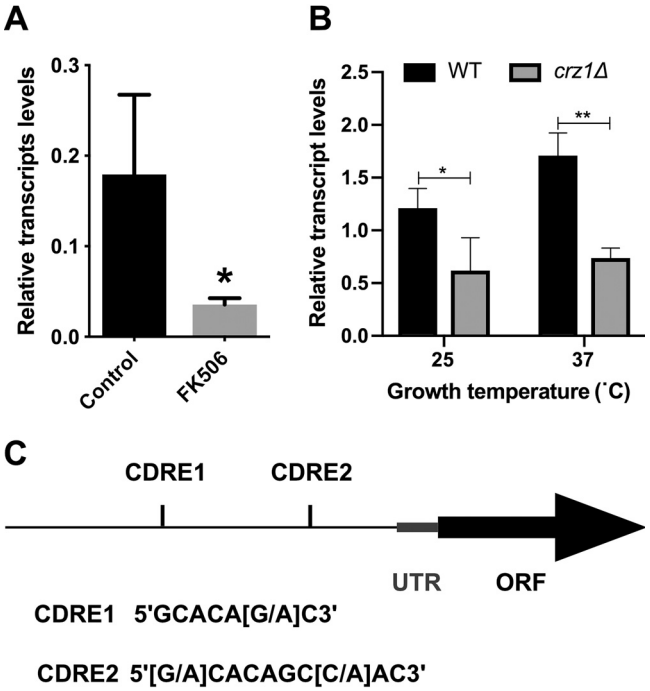

FIG 4 *NCS1* gene expression is regulated by Crz1. (A) The transcript levels of *NCS1* were determined under conditions of calcineurin inhibition. Yeast cells were incubated in YPD medium at 37°C in the absence or presence of FK506 (1 μg/ml) for 1 h. *NCS1* expression was normalized to *ACT1* transcript levels. Bars represent the means ± standard deviations (three biological replicates). Statistics were conducted using Student's *t* test (*, $P < 0.05$; ***, $P < 0.001$). (B) *NCS1* gene expression in WT and *crz1*Δ null mutant cells was assessed by RT-qPCR. Yeast cells were incubated in YPD at 25°C or 37°C for 16 h. *NCS1* expression was normalized to *ACT1* transcript levels. Each bar represents the mean ± the standard deviation (three biological triplicates). Statistical analysis was performed using Student's *t* test (*, $P < 0.05$; **, $P < 0.01$). (C) The *NCS1* regulatory sequence contains two Crz1 binding motifs (CDRE1 and CDRE2). CDRE, calcineurin-dependent response element; UTR, untranslated region; ORF, open reading frame.

model of cryptococcosis. In a Kaplan-Meier survival study, the *ncs1*Δ null mutant strain was found to be hypovirulent (median lethal time [LT_{50}], 32.7 days) compared to the WT (LT_{50}, 18.9; $P < 0.0001$) and the *ncs1*Δ::*NCS1* strain (LT_{50}, 17.4 days; $P < 0.0001$) (Fig. 5A). Although the disruption of *NCS1* prolonged mouse survival, no difference in the fungal burdens in lung and brain were observed at time of death, when infected mice had lost 20% of their preinfection weight (Fig. 5B). Thus, the *ncs1*Δ null mutant strain is capable of infecting the lung and brain tissue but potentially grows at a lower rate than the WT and the *ncs1*Δ::*NCS1* strains.

Ncs1 is necessary for growth under host-mimicking conditions. We also analyzed the capability of *ncs1*Δ mutant to synthesize the polysaccharide capsule, since this is the main cryptococcal virulence factor (1, 12). We observed that when the *ncs1*Δ strain was grown under capsule-inducing conditions (Dulbecco modified Eagle medium [DMEM] at 37°C and 5% CO_2), mutant cells produced smaller capsules than the WT and *ncs1*Δ::*NCS1* strain (Fig. 6A). However, capsule size was not affected following growth in mouse serum (data not shown). Next, we compared growth of the *ncs1*Δ mutant to that of the WT and *ncs1*Δ::*NCS1* strains under the capsule induction condition utilized and found that the null mutant growth was drastically compromised (Fig. 6B). Similarly, growth of the *ncs1*Δ strain was severely impaired in mouse serum over a 24-h period at 37°C with 5% CO_2 (Fig. 6C). Collectively, these results suggest that hypovirulence of the *ncs1*Δ mutant is most likely associated with the observed growth defects, with reduced capsule size making only a minor contribution to this virulence phenotype.

Ncs1 is important for the release of daughter cells. Microscopic analysis to evaluate the size of the polysaccharide capsule and the growth rate in mouse serum

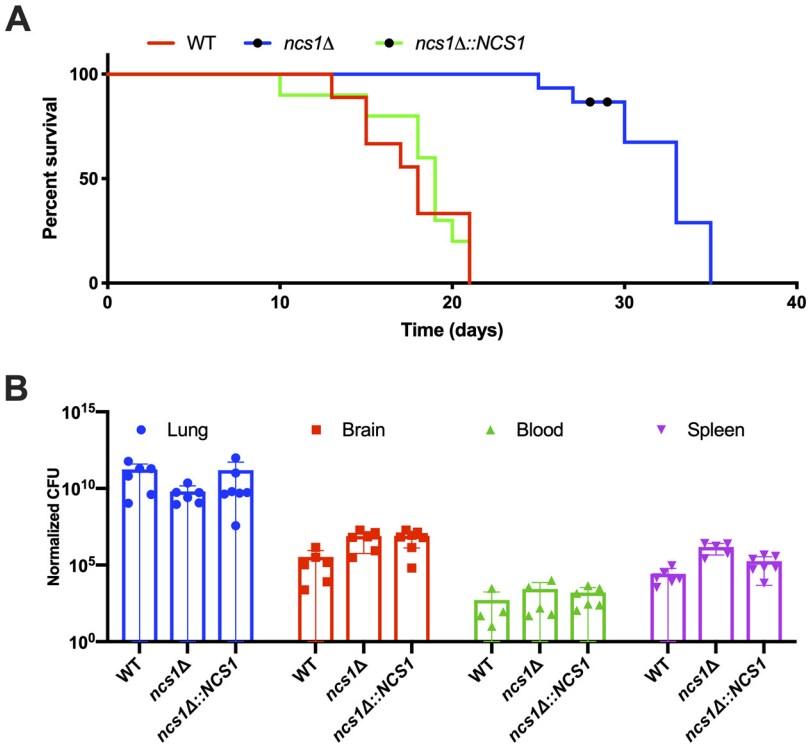

FIG 5 Ncs1 is required for full virulence in a mouse inhalation model of cryptococcosis. C57BL/6J mice (10 mice per group) were infected with 500,000 cells of the WT, *ncs1*Δ, or *ncs1*Δ::*NCS1* strain. Mice were monitored daily and euthanized by CO_2 asphyxiation when they had lost 20% of their preinfection weight. (A) Median mouse survival differences were estimated using a Kaplan-Meier log-rank Mantel-Cox test. The increase in median survival of *ncs1*Δ-infected mice relative to the other two infection groups was statistically significant ($P < 0.0001$). (B) Lungs, brain, and spleen were removed posteuthanasia, weighed, homogenized, serially diluted, and plated onto Sabouraud dextrose agar plates to determine fungal burden by quantitative culture (CFU) following 3 days of growth at 30°C. CFU were adjusted to reflect CFU/gram of tissue and CFU/milliliter of blood (normalized CFU). Statistical significance was determined using one-way ANOVA. However, no differences in organ burden were found.

revealed that some *ncs1*Δ cells displayed aberrant morphology and cell division (Fig. 7A), suggesting that Ncs1 could play a role in cell cycle progression. We therefore investigated the growth defect further by determining the time it took for buds to emerge using time-lapse microscopy (Fig. 7B and Movies S1 and S2). Given that the mutant was severely attenuated in growth when cultured in DMEM or exposed to mouse serum, we chose YPD medium for this analysis, as it is a richer medium in which mutant growth is not as compromised. To avoid bias due to lack of synchronization, we only measured the time of bud emergence in cells after the bud of the first daughter cell had separated from the mother or, in the case of the mutant cells, where progeny did not detach from mother cell, after the second bud emergence. The results demonstrate that it took ~70 min for buds to emerge in the WT cells and more than 140 min for buds to emerge in isolated and clumped *ncs1*Δ mutant cells (Fig. 7C). Furthermore, buds were slow to be released in some *ncs1*Δ mutant cells, resulting in more extensive cell clumping.

As cell division is linked to the cell cycle, we evaluated whether cells lacking *NCS1* displayed defects in cell cycle regulation by measuring the levels of two transcripts associated with different stages of the cell cycle: the G_1 cyclin encoded by *CNL1* (52) and the S phase DNA replication licensing factor encoded by *MCM2* (53, 54). We also measured the transcript levels of the G protein-coupled receptor encoded by *GPA2*, which displays oscillatory expression during the cell cycle (53, 54). All three genes were upregulated in the *ncs1*Δ strain compared to the WT after 4 h of growth in YPD (Fig. 7D), reinforcing that cell cycle progression is altered in the *ncs1*Δ mutant strain.

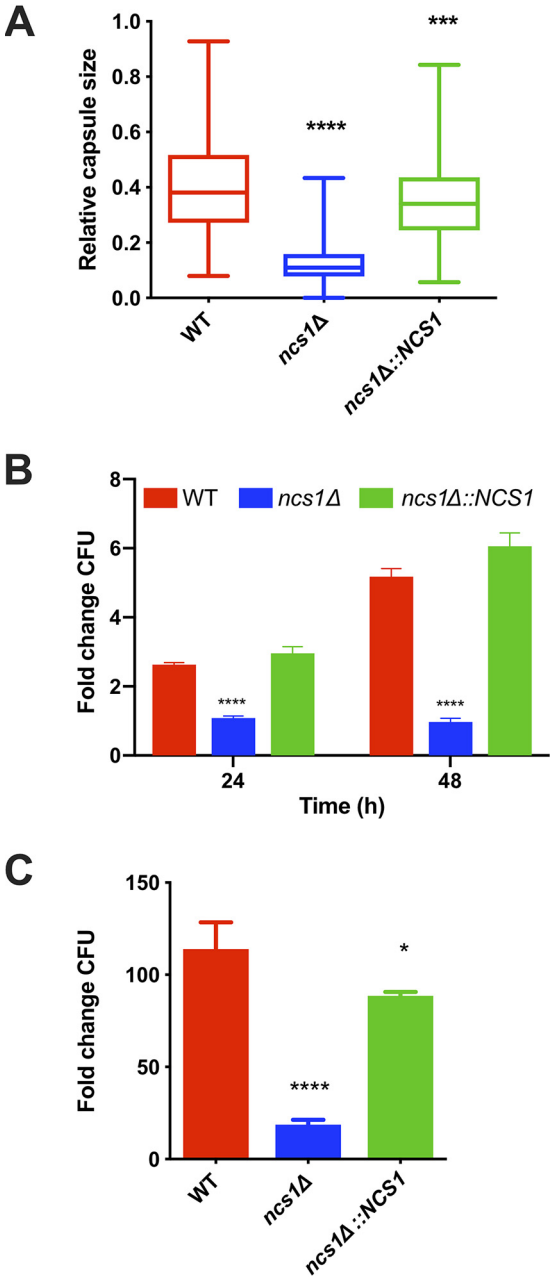

FIG 6 Ncs1 is necessary for growth under host-mimicking conditions. (A) Capsule sizes of WT, *ncs1*Δ, and *ncs1*Δ::*NCS1* cells were determined following incubation in capsule-inducing medium (DMEM) for 72 h (37°C and 5% CO_2). Capsules were visualized by India ink staining and light microscopy, and measurements were performed using ImageJ software for at least 50 cells of each strain. Relative capsule size was defined as the distance between the cell wall and the capsule outer border by cell diameter. Statistical analysis was performed using one-way ANOVA, with Tukey *post hoc* test. **** $P < 0.0001$, and ***, $P < 0.001$, compared to the WT. (B) Growth of the WT, *ncs1*Δ, and *ncs1*Δ::*NCS1* cells in DMEM (37°C and 5% CO_2) for 24 or 48 h was assessed by quantitative culture (CFU). The results represent the mean ± standard deviation (three biological replicates) of each strain normalized to the CFU of the inoculum, described as fold change. Statistical analysis was performed using one-way ANOVA with Dunnett's *post hoc* test. Significant differences compared to WT are marked (****, $P < 0.0001$). (C) Growth of the WT, *ncs1*Δ, and *ncs1*Δ::*NCS1* cells for 24 h at 37°C 5% CO_2 in heat-inactivated mouse serum was by quantitated (CFU). The results are expressed as a fold change relative to the initial inoculum (10^4 cells/ml) and represent the means ± standard deviations (three biological replicates). Statistical analysis was performed using one-way ANOVA and Dunnett's *post hoc* test (*, $P < 0.05$, and ****, $P < 0.0001$, relative to the WT).

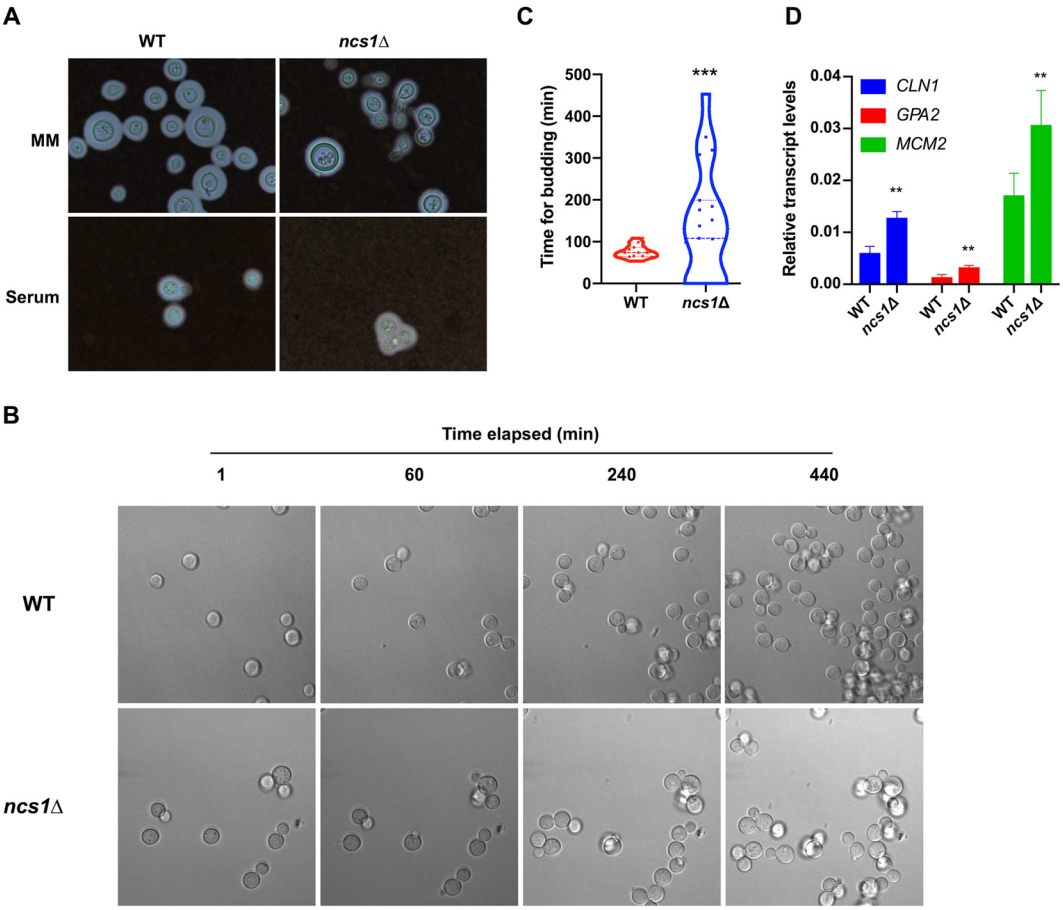

FIG 7 The *ncs1*Δ null mutant strain displays aberrant cell division and morphology (A), delayed bud emergence (B and C), and altered cell cycle regulation (D). (A) WT and *ncs1*Δ cells were grown in minimal medium for 72 h at 37°C and 5% CO_2 (upper panel) or in heat-inactivated mouse serum for 24 h at 37°C and 5% CO_2 (lower panel), stained with India ink, and visualized by light microscopy. (B and C) Fungal cells were incubated in YPD medium for 16 h inside a chamber coupled to a confocal microscope (37°C and 5% CO_2), and bud emergence time was recorded using time-lapse microscopy. Time measurements were initiated after the first round of bud emergence to avoid errors associated with the lack of synchronization. Images were acquired every 30 s. The graph in panel C represents the mean time for buds to emerge (minutes) ± standard deviation of at least 15 cells per strain. Statistical analysis was performed using the nonparametric Mann-Whitney *test* (***, $P < 0.0001$). (D) Transcript levels of genes encoding cell cycle regulators were assessed in WT and *ncs1*Δ cells by RT-qPCR. Cells were grown in YPD at 37°C for 4 h. Results represent the mean transcript levels ± standard deviations (three biological triplicates) with each gene normalized to *ACT1* transcript levels. Statistical analysis was performed using Student's *t* test (**, $P < 0.01$).

DISCUSSION

Our results indicate that *NCS1* expression in *C. neoformans* is regulated by Ca^{2+} and the calcineurin/Crz1 pathway and corroborate findings on the Ncs1 ortholog in fission yeast (35). In contrast to our conclusions and those made in studies using *S. pombe*, the *S. cerevisiae* Ncs1 ortholog, Frq1, was found to be essential for viability and the level of *FRQ1* expression was not influenced by the calcineurin/Crz1 pathway, as revealed by microarray analysis (55). This suggests that distinct calcium sensing mechanisms exist in fungal species despite widespread functional conservation of Ncs1 and other regulators of Ca^{2+} homeostasis.

An interesting feature of the *ncs1*Δ mutant is its attenuated virulence in a murine model of cryptococcosis. In contrast, attenuated virulence was not observed for the null Ncs1 ortholog mutant (*NCSA*) in *A. fumigatus* (41), reaffirming that processes regulated by Ncs1 orthologs in pathogenic fungi differ or that other genes can compensate in the absence of *NCSA*. Moreover, the cryptococcal *ncs1*Δ strain took longer to achieve the growth densities associated with debilitating infection in the tissues of WT-infected mice. This slower growth phenotype *in vivo* correlated with the reduced rate of

proliferation of the *ncs1*Δ strain in mouse serum and impaired bud emergence and release. These results confirm that Ncs1 is important for fungal adaptation to the host environment and for the establishment of disease and reaffirm the importance of Ca^{2+} homeostasis and Ca^{2+} signaling in cryptococcal virulence. Our findings also extend the set of calcium-related genes involved in virulence to include Ncs1.

Given that expression of ~40 virulence-associated genes is linked to the cell cycle in *C. neoformans*, the control of this process is fundamental to disease progression (53). In *S. cerevisiae*, Ca^{2+} homeostasis is linked to cell cycle regulation, as a decrease in intracellular Ca^{2+} leads to transient arrest in the G_1 phase, followed by interruption in the G_2/M phase (27, 56–58). Moreover, bud emergence and the cell cycle depend on calcineurin activity, which regulates the availability of proteins involved in cell cycle regulation. These proteins include Swe1, a negative regulator of Cdc28/Clb complex, Cln2, a protein kinase required for cell cycle progression, and a G_2 cyclin (27). In this context, we speculate a potential role for calcineurin signaling in cell cycle regulation in *C. neoformans*. Our new data demonstrate that Ncs1 interferes with the transcription profile of genes associated with cell cycle progression (*CLN1*, *GPA2*, and *MCM2*). Notably, overexpression of the *S. cerevisiae* G_1/S cyclin, Cln1, led to a filamentation phenotype (59). In our study, we showed that the cryptococcal *ncs1*Δ mutant was impaired in bud emergence and release, as seen in time-lapse microscopy. Furthermore, the *C. neoformans cln1*Δ mutant exhibited aberrant bud emergence and cell division and a consistent delay in budding (60), which are phenotypes also observed in cryptococcal *ncs1*Δ mutant cells. Additional experiments to confirm the impact of Ca^{2+} homeostasis on cryptococcal cell cycle regulation are necessary to support this hypothesis.

We hypothesize that Ca^{2+} excess, or even other types of stress, leads to activation of the calcineurin pathway, which ultimately drives the expression of Ncs1 in a Crz1-dependent fashion. Therefore, Ca^{2+}-activated Ncs1 would participate in a diverse array of cellular processes to cope with Ca^{2+} excess, including the regulation of cell division via its potential association with Pik1, a protein implicated in cell septation in fission yeast (61). Two lines of evidences support this hypothesis: (i) yeast Pik1 forms puncta consistent with its localization in the Golgi apparatus (62) and we observed that cryptococcal Ncs1 also forms puncta, particularly when Ca^{2+} is present, and (ii) yeast Frq1 physically interacts with Pik1 (62). Structural studies performed on Ncs1 revealed that the myristoyl group flips out following Ca^{2+} binding, allowing Ncs1 to anchor reversibly to membranes (20, 39, 40). Thus, it is possible that Ca^{2+} binding to Ncs1 exposes the hydrophobic N-myristoylation domain, promoting Ncs1 association with Pik1 in Golgi membranes and, hence, proper cell septation and division. Further experiments are required to confirm that the puncta assumed by Ncs1 upon addition of calcium colocalize with the Golgi.

In summary, we have characterized the Ncs1 homolog in *C. neoformans*, demonstrating its importance in Ca^{2+} homeostasis and virulence. We showed that in contrast to *S. cerevisiae*, *NCS1* is a calcineurin-responsive gene in *C. neoformans*, with calcineurin and Ncs1 working together to regulate calcium homeostasis and, hence, promote fungal growth and virulence. To our knowledge, this is the first report of a role for Ncs1 in fungal virulence using a mammalian infection model and of a potential correlation between Ca^{2+} signaling and cell cycle progression in *C. neoformans*.

MATERIALS AND METHODS

Fungal strains and media. *C. neoformans* serotype A strain Kn99 was chosen to conduct the study as the wild type (WT). The *NCS1* gene (CNAG_03370) deletion mutant (*ncs1*Δ), *cna1*Δ mutant, and *cam1*Δ mutant were obtained from H. Madhani's library (47). The *ncs1*Δ reconstituted strain (*ncs1*Δ::*NCS1*), the *mid1*Δ *ncs1*Δ double mutant, and the *NCS1*::*GFP* strain were all constructed using overlapping PCR as previously described (63), and site-directed homologous recombination was performed. Transformation was carried out using biolistic transformation, as previously described (64). The primer list is presented at Table S1, and the confirmations of the cassette's insertions are demonstrated in Fig. S1. Fungal cells were maintained on solid YPD medium (1% yeast extract, 2% peptone, 2% dextrose, and 1.5% agar). YPD plates containing hygromycin (200 μg/ml) or G418 (100 μg/ml) were used to select *C. neoformans* transformants.

***In silico* analysis.** To evaluate Ncs1 protein conserved domains, we used the protein sequences and annotations retrieved from the FungiDB database (http://fungidb.org) (65), applying FungiDB tools and the InterproScan database (66). The same was performed for NMT-themyrpredictor database to identify the N-terminal myristoylation consensus sequence. Conservation was assessed using BLASTp against target proteins. Finally, the presence of the Crz1-binding motif on the promoter region of the *NCS1* gene was made by manual search. We recovered the putative regulatory regions of cryptococcal genes from FungiDB (http://fungidb.org), selecting 1,000 bp upstream of the transcription start site of *NCS1* gene. The sequences utilized for Crz1-binding motif search are already described (50).

Virulence assay. Virulence assays were performed as previously described (67). Briefly, female C57BL/6 mice (10 per infection group) were anesthetized by inhalation of 3% isoflurane in oxygen and infected with 5×10^5 fungal cells (WT, *ncs1*Δ, or *ncs1*Δ::*NCS1* strain) via the nasal passages. Mice were monitored daily and euthanized by CO_2 asphyxiation when they had lost 20% of their preinfection weight or prior in the case of debilitating symptoms of infection. Median survival differences were estimated using a Kaplan-Meier log-rank Mantel-Cox test. Posteuthanasia, lungs and brain were removed, weighed, and homogenized in 2 ml of sterile phosphate-buffered saline (PBS) using a BeadBug (Benchmark Scientific). Organ homogenates were serially diluted and plated onto Sabouraud dextrose agar plates. Plates were incubated at 30°C for 2 days. Colony counts were performed and adjusted to reflect the total number of CFU per gram of tissue or milliliter of blood. For fungal burden analysis, two-way analysis of variance (ANOVA) with Tukey *post hoc* was utilized to determine the statistical significance.

***C. neoformans* replication in mouse serum.** A total of 10 BALB/c mice (10 weeks old) were obtained from Biotechnology Center, UFRGS, Brazil. Mice were anesthetized using isoflurane (in a chamber), and blood was collected from the retro-orbital space, using a glass capillary. Next, mice were euthanized using an overdose of thiopental (140 mg/kg of body weight). Serum was obtained from total blood after centrifugation (3,000 × *g* for 15 min at room temperature). A total of 1,000 cells in 100-μl suspensions of the WT, *ncs1*Δ, and *ncs1*Δ::*NCS1* strains were inoculated in heat-inactivated mouse serum in a 96-well plate and incubated at 37°C and 5% CO_2 for 24 h. Yeast cells were collected and plated on YPD plates for CFU determination. Separate wells were used for cell morphology analysis, in which yeast cells were first fixed with 4% paraformaldehyde for 30 min at 37°C and then analyzed using light microscopy.

Yeast growth in DMEM. A total of 1×10^6 cells in 1,000-μl suspensions of the WT, *ncs1*Δ, and *ncs1*Δ::*NCS1* strains were inoculated in DMEM in a 24-well plate and incubated at 37°C and 5% CO_2 for 24 and 48 h. Next, yeast cells were gathered and plated on YPD plates for CFU determination. Separate wells were used for cell morphology analysis, in which fungal cells were fixed with 4% paraformaldehyde for 30 min at 37°C and then analyzed using India ink counterstaining in light microscopy.

Intracellular calcium measurements. Free intracellular Ca^{2+} in *C. neoformans* was quantified by flow cytometry (Millipore GuavaSoft) following cellular staining with the calcium sensor dye Fluo-4-AM (Thermo Fisher Scientific) at a final concentration of 2 μM. Briefly, yeast cells were cultured overnight on YPD at 30°C with shaking. Next, cells were centrifuged (6,000 rpm for 3 min) and washed twice with PBS. After adjusting the cell density (optical density at 600 nm [OD_{600}] = 1.0), the Fluo-4-AM dye was added to each tube and incubated at 37°C for 1 h. The flow was adjusted to pass <500 cells/μl, and a total of 5,000 events were evaluated.

Phenotypic characterization. For phenotypic characterization, WT, *ncs1*Δ mutant, and *ncs1*Δ::*NCS1* complemented strains were grown overnight on YPD at 30°C with shaking. Further, cells were centrifuged, washed twice with deionized water, and adjusted to 10^8/ml. The cell suspensions were then subjected to serial dilution (10-fold), and 3 μl of each dilution was spotted onto YPD agar supplemented with different stressors, including $CaCl_2$ (200 mM and 300 mM). Cell wall perturbation was assessed using Congo red (0.1%) and calcofluor white (0.5 mg/ml), as previously described (24). The sensitivity to osmotic stress was evaluated utilizing NaCl at 1 M. Moreover, menadione (30 μM) was used as an oxidative stressor, and a low-phosphate environment was used as a starvation condition (68). All the plates were incubated for 48 h at 30°C and photographed, with the exception of plates incubated at high temperatures (37°C or 39°C).

Fluorescence and light microscopy. Fluorescence microscopy assays were accomplished using a DeltaVision fluorescence microscope. WT and *NCS1*::*GFP* cells were incubated in minimal medium (2 g/liter of L-asparagine, 1 g/liter of $MgSO_4 \cdot 7H_2O$, 6 g/liter of KH_2PO_4, 2 g/liter of thiamine) without or supplemented with 100 mM $CaCl_2$ for 16 h at 30°C with shaking. Thereafter, cells were washed once with PBS and analyzed. For light microscopy, WT, *ncs1*Δ mutant, and *ncs1*Δ::*NCS1* cells were grown in DMEM or minimal medium at 37°C and 5% CO_2 for 72 h. Next, the cells were fixed with 4% paraformaldehyde for 30 min at 37°C, washed with PBS, and then analyzed under light microscopy, using counterstaining with India ink. To define the relative capsule sizes, measures of the distance between the cell wall and the capsule outer border were determined and divided by each cell diameter through ImageJ software (https://imagej.nih.gov/ij/). At least 50 cells of each strain were measured.

Time-lapse microscopy. Cellular division was followed using confocal microscopy. The experimental design was as already described (52), with few modifications. Briefly, WT or *ncs1*Δ mutant cells were cultured overnight on liquid YPD medium at 30°C with shaking. Further, cells were washed twice with PBS and adjusted to 10^6/ml with YPD medium at pH 7.45. One hundred microliters of cell suspension was inoculated on a 35/10-mm glass-bottom cell culture dish (Greiner Bio-one). The culture dish was previously treated with 100 μl of poly-L-lysine (0.1 mg/ml) for 1 h, washed 3 times with PBS, and then incubated with 10 μg/ml of monoclonal antibody (MAb) 18B7 for 1 h. The culture dishes were incubated in a temperature-controlled microscope chamber adjusted to 37°C and 5% CO_2. Image acquisition was done in a 30-s interval, using a differential inference contrast (DIC) objective in an FV1000 confocal microscope at the Microscopy and Microanalysis Center (CMM) of the Universidade Federal do Rio

Grande do Sul (UFRGS). Statistical analysis was done by timing how long each mother cell took to originate a bud. Measurements were performed at the beginning of the second budding in order to avoid errors associated with the lack of tools to synchronize cells.

RT-qPCR analysis. For gene expression analysis, strains were subjected to different conditions, as described in the figure legends. RT-qPCR technique was performed for all experiments as follows. Cryptococcal cells were washed once with PBS, then frozen in liquid nitrogen, and lyophilized. Cell lysis was performed by vortexing the tubes with the dry pelleted cells using acid-washed glass beads (Sigma-Aldrich Co., St. Louis, MO). Three independent sets of RNA samples for each strain were prepared using TRIzol reagent (Invitrogen, Carlsbad, CA) according to the manufacturer's protocol. Next, RNA samples were treated with DNase (Promega, Madison, WI), and a total of 300 ng of treated-RNA was used for reverse transcription with ImProm-II reverse transcriptase (Promega). RT-qPCR was performed on a real-time PCR StepOne real-time PCR system (Applied Biosystems, Foster City, CA). PCR thermal cycling conditions had an initial step at 94°C for 5 min, followed by 40 cycles at 94°C for 30 s, 60°C for 30 s, and 72°C for 60 s. Platinum SYBR green qPCR Supermix (Invitrogen, Carlsbad, CA) was used as the reaction mix, with 1 μl of the cDNA (16 ng) template, in a final volume of 20 μl. Each cDNA sample was done in technical triplicates. Melting-curve analysis was performed at the end of the reaction to confirm a single PCR product. The data were normalized to the actin cDNA levels. Relative expression was determined by the threshold cycle ($2^{-\Delta CT}$) method (69).

Ethics statement. The animals were obtained from the Animal Resource Centre, Floreat Park, Western Australia, Australia. The *in vivo* procedures were performed under protocol number 4254, approved by Western Sydney Local Health District Animal Ethics Committee, accomplished according to the current guidelines of The National Health and Medical Research Council of Australia. The Animal Use Ethics Committee (CEUA/UFRGS) approved the animal experimentation under reference no. 22488.

SUPPLEMENTAL MATERIAL

Supplemental material is available online only.

MOVIE S1, MOV file, 9.9 MB.

MOVIE S2, MOV file, 1.4 MB.

FIG S1, TIF file, 1.7 MB.

FIG S2, TIF file, 1 MB.

FIG S3, TIF file, 2.4 MB.

TABLE S1, DOCX file, 0.02 MB.

ACKNOWLEDGMENTS

We are grateful to Leonardo Nimrichter, Kildare Miranda, and Augusto Schrank for helpful discussions. We also thank Hiten Madhani for providing the *ncs1*Δ, *cna1*Δ, and *cam1*Δ mutant strains, obtained from the Madhani knockout library (http://www.fgsc.net/crypto/crypto.htm), which was created using NIH funding (R01AI100272). We thank Arturo Casadevall for providing MAb 18B7.

This work was supported by grants from the Brazilian agencies Conselho Nacional de Desenvolvimento Científico e Tecnológico (CNPq), Coordenação de Aperfeiçoamento de Pessoal de Nível Superior (CAPES), and Fundação de Amparo a Pesquisa no Estado do Rio Grande do Sul (FAPERGS). CAPES fully supported the scholarship of E.D.S. in Brazil and during her studies at The Westmead Institute for Medical Research, Australia (Advanced Network of Computational Biology [RABICÓ] grant number 23038.010041/2013-13). This work was also supported by a project grant from the National Health and Medical Research Council of Australia (APP1058779) and a career development award from The Westmead Institute for Medical Research to S.L.

The funding agencies had no participation in the decision of the study subject, data collection and analysis, or submission of this work for publication.

Conceived and designed the experiments, E.D.S., C.C.S., J.T.D., and L.K.; performed the experiments, E.D.S., J.C.V.R., S.L., H.M., J.S., K.K.-F., and D.D.; analyzed the data, E.D.S., S.L., M.H.V., C.C.S., J.T.D., and L.K.; contributed reagents and materials, M.H.V., C.C.S., J.T.D., and L.K.; wrote the paper, E.D.S., J.T.D., and L.K.

REFERENCES

1. Ma H, May RC. 2009. Virulence in Cryptococcus species. Adv Appl Microbiol 67:131–190. https://doi.org/10.1016/S0065-2164(08)01005-8.
2. Park BJ, Wannemuehler KA, Marston BJ, Govender N, Pappas PG, Chiller TM. 2009. Estimation of the current global burden of cryptococcal meningitis among persons living with HIV/AIDS. AIDS 23:525–530. https://doi.org/10.1097/QAD.0b013e328322ffac.
3. Thinyane KH, Motsemme KM, Cooper VJL. 2015. Clinical presentation, aetiology, and outcomes of meningitis in a setting of high HIV and TB

prevalence. J Trop Med 2015:423161. https://doi.org/10.1155/2015/423161.
4. Rajasingham R, Smith RM, Park BJ, Jarvis JN, Govender NP, Chiller TM, Denning DW, Loyse A, Boulware RD. 2017. Global burden of disease of HIV-associated cryptococcal meningitis: an updated analysis. Physiol Behav 176:139–148.
5. Esher SK, Zaragoza O, Alspaugh JA. 2018. Cryptococcal pathogenic mechanisms: a dangerous trip from the environment to the brain. Mem Inst Oswaldo Cruz 113:e180057. https://doi.org/10.1590/0074-02760180057.
6. Djordjevic JT, Del Poeta M, Sorrell TC, Turner KM, Wright LC. 2005. Secretion of cryptococcal phospholipase B1 (PLB1) is regulated by a glycosylphosphatidylinositol (GPI) anchor. Biochem J 389:803–812. https://doi.org/10.1042/BJ20050063.
7. Siafakas AR, Sorrell TC, Wright LC, Wilson C, Larsen M, Boadle R, Williamson PR, Djordjevic JT. 2007. Cell wall-linked cryptococcal phospholipase B1 is a source of secreted enzyme and a determinant of cell wall integrity. J Biol Chem 282:37508–37514. https://doi.org/10.1074/jbc.M707913200.
8. Aaron PA, Gelli A. 2020. Harnessing the activity of the fungal metalloprotease, Mpr1, to promote crossing of nanocarriers through the blood-brain barrier. ACS Infect Dis 6:138–149. https://doi.org/10.1021/acsinfecdis.9b00348.
9. Vu K, Tham R, Uhrig JP, Thompson GR, Na Pombejra S, Jamklang M, Bautos JM, Gelli A. 2014. Invasion of the central nervous system by *Cryptococcus neoformans* requires a secreted fungal metalloprotease. mBio 5:e01101-14. https://doi.org/10.1128/mBio.01101-14.
10. Rodrigues ML, Nakayasu ES, Oliveira DL, Nimrichter L, Nosanchuk JD, Almeida IC, Casadevall A. 2008. Extracellular vesicles produced by *Cryptococcus neoformans* contain protein components associated with virulence. Eukaryot Cell 7:58–67. https://doi.org/10.1128/EC.00370-07.
11. Rodrigues ML, Pontes B, Viana NB, Deleon CM, Martinez R, Schnaar RL, Nosanchuk JD, Nimrichter L. 2020. Host membrane glycosphingolipids and lipid microdomains facilitate *Histoplasma capsulatum* internalization by macrophages. Cell Microbiol 21:1–31.
12. McClelland EE, Bernhardt P, Casadevall A. 2006. Estimating the relative contributions of virulence factors for pathogenic microbes. Infect Immun 74:1500–1504. https://doi.org/10.1128/IAI.74.3.1500-1504.2006.
13. Tucker SC, Casadevall A. 2002. Replication of *Cryptococcus neoformans* in macrophages is accompanied by phagosomal permeabilization and accumulation of vesicles containing polysaccharide in the cytoplasm. Proc Natl Acad Sci U S A 99:3165–3170. https://doi.org/10.1073/pnas.052702799.
14. Levitz SM, Nong SH, Seetoo KF, Harrison TS, Speizer RA, Simons ER. 1999. *Cryptococcus neoformans* resides in an acidic phagolysosome of human macrophages. Infect Immun 67:885–890. https://doi.org/10.1128/IAI.67.2.885-890.1999.
15. Charlier C, Nielsen K, Daou S, Brigitte M, Chretien F, Dromer F. 2009. Evidence of a role for monocytes in dissemination and brain invasion by *Cryptococcus neoformans*. Infect Immun 77:120–127. https://doi.org/10.1128/IAI.01065-08.
16. Cui J, Kaandorp JA, Sloot PMA, Lloyd CM, Filatov MV. 2009. Calcium homeostasis and signaling in yeast cells and cardiac myocytes. FEMS Yeast Res 9:1137–1147. https://doi.org/10.1111/j.1567-1364.2009.00552.x.
17. Cui J, Kaandorp JA, Ositelu OO, Beaudry V, Knight A, Nanfack YF, Cunningham KW. 2009. Simulating calcium influx and free calcium concentrations in yeast. Cell Calcium 45:123–132. https://doi.org/10.1016/j.ceca.2008.07.005.
18. Odom A, Del Poeta M, Perfect J, Heitman J. 1997. The immunosuppressant FK506 and its nonimmunosuppressive analog L- 685,818 are toxic to *Cryptococcus neoformans* by inhibition of a common target protein. Antimicrob Agents Chemother 41:156–161. https://doi.org/10.1128/AAC.41.1.156.
19. Francois JM. 2016. Cell surface interference with plasma membrane and transport processes in yeasts. Adv Exp Med Biol 892:11–31. https://doi.org/10.1007/978-3-319-25304-6_2.
20. Burgoyne RD. 2004. The neuronal calcium-sensor proteins. Biochim Biophys Acta 1742:59–68. https://doi.org/10.1016/j.bbamcr.2004.08.008.
21. Parys JB, De Smedt H. 2012. Inositol 1,4,5-trisphosphate and its receptors. Adv Exp Med Biol 740:255–279. https://doi.org/10.1007/978-94-007-2888-2_11.
22. Cruz MC, Fox DS, Heitman J. 2001. Calcineurin is required for hyphal elongation during mating and haploid fruiting in *Cryptococcus neoformans*. EMBO J 20:1020–1032. https://doi.org/10.1093/emboj/20.5.1020.
23. Kozubowski L, Lee SC, Heitman J. 2011. Signalling pathways in the pathogenesis of *Cryptococcus*. Cell Microbiol 23:1–7.
24. Lev S, Desmarini D, Chayakulkeeree M, Sorrell TC, Djordjevic JT. 2012. The Crz1/Sp1 transcription factor of *Cryptococcus neoformans* is activated by calcineurin and regulates cell wall integrity. PLoS One 7:e51403. https://doi.org/10.1371/journal.pone.0051403.
25. Odom A, Muir S, Lim E, Toffaletti DL, Perfect J, Heitman J. 1997. Calcineurin is required for virulence of *Cryptococcus neoformans*. EMBO J 16:2576–2589. https://doi.org/10.1093/emboj/16.10.2576.
26. Park HS, Chow EWL, Fu C, Soderblom EJ, Moseley MA, Heitman J, Cardenas ME. 2016. Calcineurin targets involved in stress survival and fungal virulence. PLoS Pathog 12:e1005873. https://doi.org/10.1371/journal.ppat.1005873.
27. Miyakawa T, Mizunuma M. 2007. Physiological roles of calcineurin in *Saccharomyces cerevisiae* with special emphasis on its roles in G2/M cell-cycle regulation. Biosci Biotechnol Biochem 71:633–645. https://doi.org/10.1271/bbb.60495.
28. Carafoli E, Santella L, Branca D, Brini M. 2001. Generation, control, and processing of cellular calcium signals. Crit Rev Biochem Mol Biol 36:107–260. https://doi.org/10.1080/20014091074183.
29. Liu M, Du P, Heinrich G, Cox GM, Gelli A. 2006. Cch1 mediates calcium entry in *Cryptococcus neoformans* and is essential in low-calcium environments. Eukaryot Cell 5:1788–1796. https://doi.org/10.1128/EC.00158-06.
30. Fan W, Idnurm A, Breger J, Mylonakis E, Heitman J. 2007. Ecal, a sarcoplasmic/endoplasmic reticulum Ca2+-ATPase, is involved in stress tolerance and virulence in *Cryptococcus neoformans*. Infect Immun 75:3394–3405. https://doi.org/10.1128/IAI.01977-06.
31. Kmetzsch L, Staats CC, Simon E, Fonseca FL, de Oliveira DL, Sobrino L, Rodrigues J, Leal AL, Nimrichter L, Rodrigues ML, Schrank A, Vainstein MH. 2010. The vacuolar Ca^{2+} exchanger Vcx1 is involved in calcineurin-dependent Ca^{2+} tolerance and virulence in *Cryptococcus neoformans*. Eukaryot Cell 9:1798–1805. https://doi.org/10.1128/EC.00114-10.
32. Kmetzsch L, Staats CC, Cupertino JB, Fonseca FL, Rodrigues ML, Schrank A, Vainstein MH. 2013. The calcium transporter Pmc1 provides Ca^{2+} tolerance and influences the progression of murine cryptococcal infection. FEBS J 280:4853–4864. https://doi.org/10.1111/febs.12458.
33. Squizani ED, Oliveira NK, Reuwsaat JCV, Marques BM, Lopes W, Gerber AL, de Vasconcelos ATR, Lev S, Djordjevic JT, Schrank A, Vainstein MH, Staats CC, Kmetzsch L. 2018. Cryptococcal dissemination to the central nervous system requires the vacuolar calcium transporter Pmc1. Cell Microbiol 20:e12803. https://doi.org/10.1111/cmi.12803.
34. Hamasaki-Katagiri N, Molchanova T, Takeda K, Ames JB. 2004. Fission yeast homolog of neuronal calcium sensor-1 (Ncs1p) regulates sporulation and confers calcium tolerance. J Biol Chem 279:12744–12754. https://doi.org/10.1074/jbc.M311895200.
35. Hamasaki-Katagiri N, Ames JB. 2010. Neuronal calcium sensor-1 (Ncs1p) is up-regulated by calcineurin to promote Ca^{2+} tolerance in fission yeast. J Biol Chem 285:4405–4414. https://doi.org/10.1074/jbc.M109.058594.
36. Fan Y, Ortiz-Urquiza A, Kudia RA, Keyhani NO. 2012. A fungal homologue of neuronal calcium sensor-1, Bbcsa1, regulates extracellular acidification and contributes to virulence in the entomopathogenic fungus Beauveria bassiana. Microbiology (Reading) 158:1843–1851. https://doi.org/10.1099/mic.0.058867-0.
37. Gohain D, Deka R, Tamuli R. 2016. Identification of critical amino acid residues and functional conservation of the *Neurospora crassa* and *Rattus norvegicus* orthologues of neuronal calcium sensor-1. Genetica 144:665–674. https://doi.org/10.1007/s10709-016-9933-y.
38. Saitoh KI, Arie T, Teraoka T, Yamaguchi I, Kamakura T. 2003. Targeted gene disruption of the neuronal calcium sensor 1 homologue in rice blast fungus, *Magnaporthe grisea*. Biosci Biotechnol Biochem 67:651–653. https://doi.org/10.1271/bbb.67.651.
39. Tamuli R, Kumar R, Deka R. 2011. Cellular roles of neuronal calcium sensor-1 and calcium/calmodulin-dependent kinases in fungi. J Basic Microbiol 51:120–128. https://doi.org/10.1002/jobm.201000184.
40. Ames JB, Hendricks KB, Strahl T, Huttner IG, Hamasaki N, Thorner J. 2000. Structure and calcium-binding properties of Frq1, a novel calcium sensor in the yeast *Saccharomyces cerevisiae*. Biochemistry 39:12149–12161. https://doi.org/10.1021/bi0012890.
41. Mota Júnior AO, Malavazi I, Soriani FM, Heinekamp T, Jacobsen I, Brakhage AA, Savoldi M, Goldman MHS, Da Silva Ferreira ME, Goldman GH. 2008. Molecular characterization of the *Aspergillus fumigatus* NCS-1

homologue, NcsA. Mol Genet Genomics 280:483–495. https://doi.org/10.1007/s00438-008-0381-y.
42. Kraus PR, Nichols CB, Heitman J. 2005. Calcium- and calcineurin-independent roles for calmodulin in *Cryptococcus neoformans* morphogenesis and high-temperature growth. Eukaryot Cell 4:1079–1087. https://doi.org/10.1128/EC.4.6.1079-1087.2005.
43. Lemire S, Jeromin A, Boisselier É. 2016. Membrane binding of neuronal calcium sensor-1 (NCS1). Colloids Surf B Biointerfaces 139:138–147. https://doi.org/10.1016/j.colsurfb.2015.11.065.
44. Burgoyne RD. 2007. Neuronal calcium sensor proteins: generating diversity in neuronal Ca^{2+} signalling. Nat Rev Neurosci 8:182–125. https://doi.org/10.1038/nrn2093.
45. Udenwobele DI, Su R, Good SV, Ball TB. 2017. Myristoylation: an important protein modification in the immune response. Front Immunol 8:751. https://doi.org/10.3389/fimmu.2017.00751.
46. Kraus PR, Heitman J. 2003. Coping with stress: calmodulin and calcineurin in model and pathogenic fungi. Biochem Biophys Res Commun 311:1151–1157. https://doi.org/10.1016/s0006-291x(03)01528-6.
47. Liu OW, Chun CD, Chow ED, Chen C, Madhani HD, Noble SM. 2008. Systematic genetic analysis of virulence in the human fungal pathogen *Cryptococcus neoformans*. Cell 135:174–177. https://doi.org/10.1016/j.cell.2008.07.046.
48. Vu K, Bautos JM, Gelli A. 2015. The Cch1-Mid1 high-affinity calcium channel contributes to the virulence of *Cryptococcus neoformans* by mitigating oxidative stress. Eukaryot Cell 14:1135–1143. https://doi.org/10.1128/EC.00100-15.
49. Hong MP, Vu K, Bautos JM, Tham R, Jamklang M, Uhrig JP, Gelli A. 2013. Activity of the calcium channel pore Cch1 is dependent on a modulatory region of the subunit Mid1 in *Cryptococcus neoformans*. Eukaryot Cell 12:142–150. https://doi.org/10.1128/EC.00130-12.
50. Chow EWL, Clancey SA, Billmyre RB, Averette AF, Granek JA, Mieczkowski P, Cardenas ME, Heitman J. 2017. Elucidation of the calcineurin-Crz1 stress response transcriptional network in the human fungal pathogen *Cryptococcus neoformans*. PLoS Genet 13:e1006667. https://doi.org/10.1371/journal.pgen.1006667.
51. Liu S, Hou Y, Liu W, Lu C, Wang W, Sun S. 2015. Components of the calcium-calcineurin signaling pathway in fungal cells and their potential as antifungal targets. Eukaryot Cell 14:324–334. https://doi.org/10.1128/EC.00271-14.
52. García-Rodas R, Cordero RJB, Trevijano-Contador N, Janbon G, Moyrand F, Casadevall A, Zaragoza O. 2014. Capsule growth in *Cryptococcus neoformans* is coordinated with cell cycle progression. mBio 5:e00945-14. https://doi.org/10.1128/mBio.00945-14.
53. Kelliher CM, Haase SB. 2017. Connecting virulence pathways to cell-cycle progression in the fungal pathogen *Cryptococcus neoformans*. Curr Genet 63:803–811. https://doi.org/10.1007/s00294-017-0688-5.
54. Kelliher CM, Leman AR, Sierra CS, Haase SB. 2016. Investigating conservation of the cell-cycle-regulated transcriptional program in the fungal pathogen, *Cryptococcus neoformans*. PLoS Genet 12:e1006453. https://doi.org/10.1371/journal.pgen.1006453.
55. Yoshimoto H, Saltsman K, Gasch AP, Li HX, Ogawa N, Botstein D, Brown PO, Cyert MS. 2002. Genome-wide analysis of gene expression regulated by the calcineurin/Crz1p signaling pathway in *Saccharomyces cerevisiae*. J Biol Chem 277:31079–31088. https://doi.org/10.1074/jbc.M202718200.
56. Kahl CR, Means AR. 2003. Regulation of cell cycle progression by calcium/calmodulin-dependent pathways. Endocr Rev 24:719–736. https://doi.org/10.1210/er.2003-0008.
57. Zhang YQ, Rao R. 2008. A spoke in the wheel: calcium spikes disrupt yeast cell cycle. Cell Cycle 7:870–873. https://doi.org/10.4161/cc.7.7.5616.
58. Iida H, Sakaguchi S, Yagawa Y, Anraku Y. 1990. Cell cycle control by Ca2+ in *Saccharomyces cerevisiae*. J Biol Chem 265:21216–21222.
59. Kron SJ, Gow NA. 1995. Budding yeast morphogenesis: signalling, cytoskeleton and cell cycle. Curr Opin Cell Biol 7:845–855. https://doi.org/10.1016/0955-0674(95)80069-7.
60. Virtudazo EV, Kawamoto S, Ohkusu M, Aoki S, Sipiczki M, Takeo K. 2010. The single Cdk1-G1 cyclin of *Cryptococcus neoformans* is not essential for cell cycle progression, but plays important roles in the proper commitment to DNA synthesis and bud emergence in this yeast. FEMS Yeast Res 10:605–618. https://doi.org/10.1111/j.1567-1364.2010.00633.x.
61. Park J, Steinbach SK, Desautels M, Hemmingsen SM. 2009. Essential role for *Schizosaccharomyces pombe* pik1 in septation. PLoS One 4:e6179. https://doi.org/10.1371/journal.pone.0006179.
62. Strahl T, Hama H, Dewald DB, Thorner J. 2005. Yeast phosphatidylinositol 4-kinase, Pik1, has essential roles at the Golgi and in the nucleus. J Cell Biol 171:967–979. https://doi.org/10.1083/jcb.200504104.
63. Lev S, Desmarini D, Li C, Chayakulkeeree M, Traven A, Sorrell TC, Djordjevic JT. 2013. Phospholipase C of *Cryptococcus neoformans* regulates homeostasis and virulence by providing inositol trisphosphate as a substrate for Arg1 kinase. Infect Immun 81:1245–1255. https://doi.org/10.1128/IAI.01421-12.
64. Toffaletti DL, Rude TH, Johnston SA, Durack DT, Perfect JR. 1993. Gene transfer in *Cryptococcus neoformans* by use of biolistic delivery of DNA. J Bacteriol 175:1405–1411. https://doi.org/10.1128/jb.175.5.1405-1411.1993.
65. Basenko EY, Pulman JA, Shanmugasundram A, Harb OS, Crouch K, Starns D, Warrenfeltz S, Aurrecoechea C, Stoeckert CJ, Kissinger JC, Roos DS, Hertz-Fowler C. 2018. FungiDB: an integrated bioinformatic resource for fungi and oomycetes. J Fungi (Basel) 4:39. https://doi.org/10.3390/jof4010039.
66. Mitchell A, Chang H, Daugherty L, Fraser M, Hunter S, Lopez R, Mcanulla C, Mcmenamin C, Nuka G, Pesseat S, Sangrador-Vegas A, Scheremetjew M, Rato C, Yong S, Bateman A, Punta M, Attwood TK, Sigrist CJA, Redaschi N, Rivoire C, Xenarios I, Kahn D, Guyot D, Bork P, Letunic I, Gough J, Oates M, Haft D, Huang H, Natale DA, Wu CH, Orengo C, Sillitoe I, Mi H, Thomas PD, Finn RD. 2015. The InterPro protein families database: the classification resource after 15 years. Nucleic Acids Res 43:213–221.
67. Lev S, Li C, Desmarini D, Saiardi A, Fewings NL, Schibeci SD, Sharma R, Sorrell TC, Djordjevic JT. 2015. Fungal inositol pyrophosphate IP7 is crucial for metabolic adaptation to the host environment and pathogenicity. mBio 6:e00531-15. https://doi.org/10.1128/mBio.00531-15.
68. Lev S, Rupasinghe T, Desmarini D, Kaufman K, Sorrell TC, Roessner U, Teresa J, Id D. 2019. The PHO signaling pathway directs lipid remodeling in *Cryptococcus neoformans* via DGTS synthase to recycle phosphate during phosphate deficiency. PLoS One 14:e0212651. https://doi.org/10.1371/journal.pone.0212651.
69. Livak KJ, Schmittgen TD. 2001. Analysis of relative gene expression data using real-time quantitative PCR and the $2^{-\Delta\Delta CT}$ method. Methods 25:402–408. https://doi.org/10.1006/meth.2001.1262.